

Live-Cell Imaging of Single Receptor Composition Using Zero-Mode Waveguide Nanostructures

Christopher I. Richards,^{†,‡} Khai Luong,[§] Rahul Srinivasan,[†] Stephen W. Turner,[§] Dennis A. Dougherty,^{||} Jonas Korlach,[§] and Henry A. Lester^{*,†}

[†]Division of Biology 156-29 and ^{||}Division of Chemistry & Chemical Engineering 164-30, California Institute of Technology, 1200 East California Boulevard, Pasadena, California 91125, United States

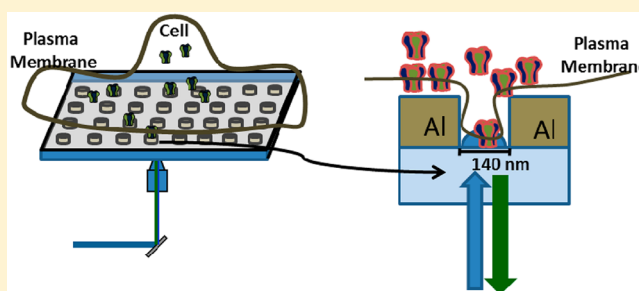
[‡]Department of Chemistry, University of Kentucky, Chemistry-Physics Building, Lexington, Kentucky 40506, United States

[§]Pacific Biosciences, 1380 Willow Road, Menlo Park, California 94025, United States

S Supporting Information

ABSTRACT: We exploit the optical and spatial features of subwavelength nanostructures to examine individual receptors on the plasma membrane of living cells. Receptors were sequestered in portions of the membrane projected into zero-mode waveguides. Using single-step photobleaching of green fluorescent protein incorporated into individual subunits, the resulting spatial isolation was used to measure subunit stoichiometry in $\alpha 4\beta 4$ and $\alpha 4\beta 2$ nicotinic acetylcholine and P2X2 ATP receptors. We also show that nicotine and cytosine have differential effects on $\alpha 4\beta 2$ stoichiometry.

KEYWORDS: Membrane receptors, nanostructures, single-molecule imaging, nicotinic receptors, zero-mode waveguide



The advent of single-molecule imaging techniques has provided insight into the dynamics of many complex biological systems,^{1–6} including membrane proteins. Advances in fluorescence-based imaging techniques have allowed for studying structural and dynamic characteristics of ion channels, receptors, and transporters.⁷ However, single-molecule measurements of membrane receptors continue to be challenged by three major factors: diffusion of proteins at the surface of the cell (as revealed by single-particle tracking), natural accumulations of membrane receptors at local densities of 10–10 000 per μm^2 , and high levels of autofluorescence.^{8,9} Studies utilizing existing imaging techniques, such as total internal reflection fluorescence (TIRF), are best suited to densities on the order of one per 1–10 μm^2 or 2–5 orders of magnitude less than typical physiological densities.

One path to mitigate the challenge of high receptor densities is to control the expression in the biological system of interest. Recent studies have utilized expression in *Xenopus laevis* oocytes, which produced the required low densities of membrane proteins that also exhibited limited diffusion. This provided the means to detect single-molecule bleaching steps of green fluorescent protein (GFP) labels associated with individual subunits.¹⁰ Furthermore, fluorescent unnatural amino acid side chains can readily be incorporated into oocytes, expanding studies to include more favorable fluorophores.¹¹ These studies and subsequent examples of similar experiments in mammalian cells¹² have demonstrated the power of single-molecule techniques to determine the stoichiometry of membrane receptors. However, applications

for these techniques remain limited primarily due to receptor diffusion and because oocytes lack some cellular machinery present in mammalian cells. These methods often control protein densities but fail to limit receptor diffusion or aggregation at the plasma membrane. While TIRF microscopy limits the excitation volume in the axial direction (200 nm), intracellular organelles are still visible¹³ leading to high background fluorescence which further complicates single-molecule measurements.

Alternatively, the utilization of zero-mode waveguide (ZMW) nanostructures has shown promise for single-molecule applications near physiological concentrations.^{14–17} ZMWs are subwavelength holes constructed in a ~ 100 nm layer of aluminum mounted on top of a glass substrate¹⁸ (Figure 1, Supporting Information). In addition to providing a rapidly attenuating evanescent field in the axial direction, the ZMW also restricts the lateral dimensions of the excitation volume to the size of the well. Single-molecule experiments of membrane receptors with ZMWs should offer two key advantages: ZMWs spatially isolate a small number (one to a few) of receptors allowing single-molecule measurement at or near physiological densities by limiting diffusion and aggregation and reducing background fluorescence from nearby molecules. In fact previous studies have shown that cell membranes can extend into the ZMWs, allowing the detection of fluctuations

Received: April 20, 2012

Revised: June 2, 2012

Published: June 5, 2012

associated with diffusion of fluorescent lipids¹⁹ and membrane resident proteins.^{14,20}

Nicotinic acetylcholine receptors (nAChRs) are an important class of cation-selective transmembrane receptor channels that express throughout the central and peripheral nervous systems and are assembled from various subunits ($\alpha 1$ – $\alpha 10$ and $\beta 2$ – $\beta 4$).²¹ The correct assembly of α and β subunits into pentameric structures is essential for proper subcellular localization, agonist sensitivity, and ion channel Ca^{2+} permeability.^{22,23} The identity and stoichiometry of subunits in each nAChR are important factors in regulating intracellular receptor processing and trafficking. To date, TIRF-based experiments with single-receptor resolution in mammalian cells have been limited to $\alpha 7$ homomeric nAChRs, which are capable of binding fluorescently labeled α -bungarotoxin.¹² The ability to directly interrogate the subunit stoichiometry of heteromeric neuronal nAChRs in living mammalian cells has not been reported.

We achieve spatial isolation of nanometer scale membrane areas within living cells by directly culturing Neuro-2a (N2a) neuroblastoma cells on ZMW arrays with defined diameters from 85 to 200 nm, corresponding to a 5.5-fold range in the membrane area that can potentially enter each ZMW (Figure 1). These cells grow neurite-like projections and generate large

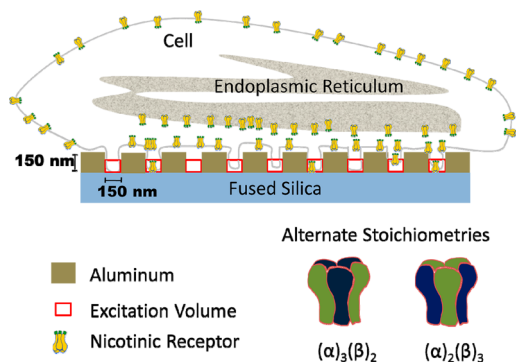


Figure 1. Membrane projection into ZMWs. Schematic of a cell plated directly on the array with extensions of small portions of the membrane protruding into ZMWs. The schematic exaggerates the well size relative to spacing, in order to illustrate the entry of the cell membrane into the wells. An individual cell typically covers 75–100 wells. The excitation volume extends ~ 50 nm into the wells creating a ~ 250 zl excitation volume for a 120 nm ZMW, as depicted by the red squares (see Supporting Information). Only a few nAChRs in the plasma membrane enter wells, probably in filopodia. Under many circumstances, the ER and other organelles contain a majority of the cell's nAChRs, but these do not enter wells. The diagram of the receptors illustrates that nicotinic receptors can potentially assemble into two stoichiometries: $\alpha_3\beta_2$ or $\alpha_2\beta_3$.

numbers of filopodia which may protrude into ZMWs making them ideally suited for the imaging of membrane resident proteins in ZMWs. Additionally, these cells do not contain endogenous nAChRs, which makes them suitable for the study of receptor assembly.²⁴ Imaging of cells transfected with plasma membrane localized monomeric cherry marker (PM-mcherry) showed that transfected cells rest directly above the ZMWs (Figure 2, Supporting Information). Importantly, we observed mcherry fluorescence in numerous adjacent ZMWs where the pattern created by the fluorescent wells resembled the footprint of cells cultured on a glass coverslip (Figure 2A,B). Clearly, the filopodia-like extensions can extend into ZMWs. This provides

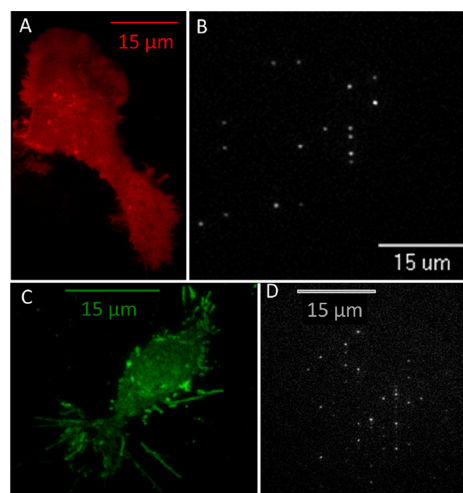


Figure 2. Isolation of membrane receptors in ZMWs. (A) N2a cells plated on a glass coverslip transfected with a PM-mcherry imaged with TIRF microscopy, illustrating the extent of membrane expression in both the soma and the processes. (B) N2a cells cultured directly on the ZMW array and transfected with the same membrane marker as in (A) and imaged from the glass side of the array. Fluorescent spots indicate the portions of the membrane containing the PM-mcherry marker that have entered the ZMW and lie within the excitation volume. (C) N2a cells plated on a glass coverslip transfected with $\alpha 4$ -GFP $\beta 4$ -wt and imaged with TIRF microscopy. The image shows that $\alpha 4\beta 4$ nAChRs are primarily localized on the plasma membrane¹³ and also shows the presence of many filopodia (5–15 μm in length) containing fluorescent nAChRs. (D) N2a cells cultured directly on the array and transfected in the same manner as in (C). Fluorescent spots indicate that portions of the membrane, probably filopodia, containing fluorescently labeled $\alpha 4\beta 4$ nAChRs extend into the ZMWs. The size of the pattern made by the fluorescent wells is consistent with the size of a typical cell.

evidence that these nanostructures are capable of isolating small segments of the membrane which contain fluorescent protein markers.

We utilized ZMW-mediated optical confinement to determine the stoichiometry of ligand-gated receptor channels. Integrating nanostructure-based imaging with the conventional tactic of observing single-molecule bleaching steps¹⁰ provided the capability to examine individual fluorescent protein-tagged subunits in heteromeric nAChRs. We previously achieved physiologically relevant plasma membrane densities (50–100/ μm^2 based on TIRF measurements) of fluorescent $\alpha 4\beta 4$ nAChRs by transfection in N2a cells.¹³ We therefore considered this system well-suited for initial analyses on subunit fluorescence of assembled receptors in ZMWs. The relatively high concentration of nAChRs at the cell membrane increases the probability that GFP-labeled nAChRs will extend into the subwavelength nanostructures. Because the fluorescent protein is incorporated in the M3–M4 loop of all nAChRs and the evanescent excitation field only extends 50 nm into the wells, all visualized individual receptors are completely within the bottom half of the well. Additionally, only assembled pentameric receptors are trafficked from the endoplasmic reticulum (ER) to the plasma membrane.^{13,25} Thus, measurements of stoichiometry in these experiments are restricted to assembled receptors at the plasma membrane. The footprint of nAChR fluorescence in transfected N2a cells plated on standard glass coverslips resembles the shape and pattern of fluorescent wells for cells transfected on ZMW arrays (Figure 2C,D). Even

at the same density that yields a clear ensemble fluorescence signal (Figure 2C) with no discernible single-molecule features in TIRF, expression on ZMWs of >144 nm diameter leads to the observation of individual receptors exhibiting GFP fluorescence. Roughly half the number of wells that exhibit PM-mcherry signals, which are associated with the penetration of the cell membrane into ZMWs, show GFP fluorescence.

The time course of fluorescence intensity from an individual ZMW can be analyzed to measure the number of GFP molecules resident in that ZMW. While $\alpha 4$ and $\beta 4$ subunits are known to coexpress in the medial habenula and may participate in some behavioral responses to nicotine, little is known about the stoichiometry of their assembly. We conducted experiments with either $\alpha 4$ -GFP + unlabeled (wt) $\beta 4$ or unlabeled $\alpha 4$ + $\beta 4$ -GFP. Because a single GFP molecule is genetically encoded into each labeled subunit, individual bleaching steps in the fluorescence intensity level indicate one subunit. On each ZMW array, 10–20% of the fluorescent wells showed bleaching events consistent with single receptors; a similar percentage of informative puncta is generally observed in TIRF-based studies of ion channels.²⁶ The remaining 80% of the wells exhibit fluorescence decays not consistent with individual molecules (see Supporting Information). The accumulated data for $\alpha 4$ -GFP + $\beta 4$ revealed that ~80% of the individually isolated receptors exhibited three bleaching steps, while ~20% exhibited two bleaching steps (Figure 3A,B). Three bleaching steps correspond to $(\alpha 4)_3(\beta 4)_2$ subunit stoichiometry, while two bleaching steps correspond to the complementary $(\alpha 4)_2(\beta 4)_3$ stoichiometry. When we studied nAChRs formed from $\alpha 4$ +

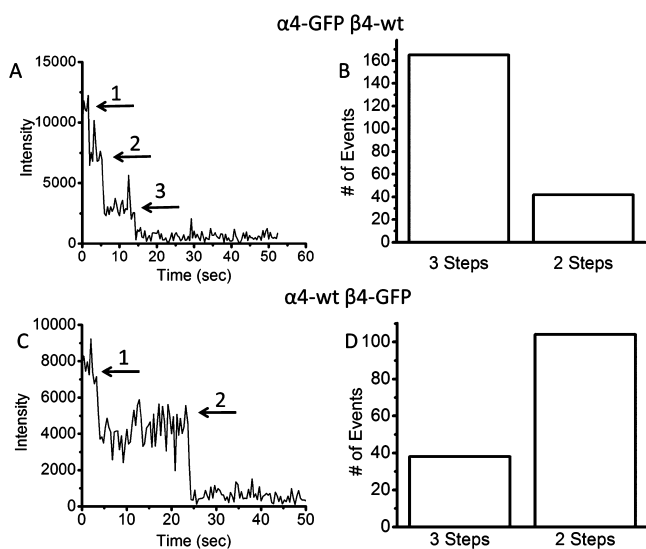


Figure 3. Single-step bleaching of labeled subunits in N2a cells cultured on ZMW arrays. (A) Time course of fluorescence intensity from a ZMW in a dish containing N2a cells transfected with $\alpha 4$ -GFP + $\beta 4$ -wt. The trace shows three bleaching steps as indicated by the arrows. The different fluorescence levels are separated by clear steps until all the GFP molecules bleach to the background level. (B) Number of three- and two-step bleaching events observed for $\alpha 4$ -GFP + $\beta 4$ -wt showing predominantly three bleaching steps. This indicates primarily $(\alpha 4)_3(\beta 4)_2$ stoichiometry. (C) Time course of fluorescence intensity from a well in a dish transfected with $\alpha 4$ -wt + $\beta 4$ -GFP. The time trace shows two bleaching steps as indicated by the arrows. (D) Number of three- and two-step bleaching events observed for $\alpha 4$ -wt + $\beta 4$ -GFP showing predominantly two bleaching steps. This also indicates primarily $(\alpha 4)_3(\beta 4)_2$ stoichiometry.

$\beta 4$ -GFP subunits, we found that <30% of the wells had three bleaching steps; 70% had two bleaching steps (Figure 3C,D). These two independent data sets indicate that the majority of $\alpha 4\beta 4$ receptors assemble in a stoichiometry of $(\alpha 4)_3(\beta 4)_2$. The complementary stoichiometry of $(\alpha 4)_2(\beta 4)_3$ occurs at a lower frequency (20–30%). The self-consistent nature of these results, using either labeled $\alpha 4$ or $\beta 4$, rules out many possible artifacts, such as undetectable bleaching of the initial fluorophore or disassembly of the heteropentamer. The majority of the noninformative fluorescent ZMWs exhibited an exponential decay with no discernible steps (70% of wells), indicating either the presence of multiple receptors or transitions obscured by fluorophore blinking (Figure 3, Supporting Information). A small fraction (10%) of the wells that exhibited step-like photobleaching was best fit to a single step. This is most likely due to simultaneous bleaching of two fluorophores (see Supporting Information).

We also validated our stoichiometry results by showing consistency with an ion channel of known subunit number. P2X2 receptors are known to assemble as trimers.²⁷ In studies on P2X2-GFP receptors, we observed 3 bleaching steps in 85% of measurable wells (Figure 4, Supporting Information).

While studies of $\alpha 4\beta 4$ illustrate the suitability of this ZMW-based method to determine the previously unknown stoichiometry of a subtype of heteromeric receptor, we also examined the more widely expressed $\alpha 4\beta 2$ nAChRs to demonstrate that the ZMW-based method can detect pharmacologically induced changes in stoichiometry. Chronic exposure to nicotine and other nAChR ligands upregulates $\alpha 4\beta 2$ nAChR density on the plasma membrane of neurons and cultured cell lines;^{28–30} upregulation may underlie both nicotine dependence and the apparent neuroprotective effect of nicotine in Parkinson's disease.²³ Upregulation is suggested to proceed via pharmacological chaperoning,^{13,31–35} and indirect evidence suggests that upregulation also involves changes in the stoichiometry of plasma membrane $\alpha 4\beta 2$ nAChRs.^{30,34} Most $\alpha 4\beta 2$ receptors are retained intracellularly, which complicates biochemical attempts to demonstrate altered plasma membrane stoichiometry. Additionally, the large population of intracellular receptors produces intolerably high background in TIRF-based measurements of plasma membrane resident receptors. We applied the ZMW measurements to $\alpha 4$ -GFP $\beta 2$ -wt nAChRs. In the absence of applied drug, we rarely detected $\alpha 4\beta 2$ nAChR in ≤ 144 nm diameter ZMWs. However, the increased area provided by the larger ZMWs (~200 nm diameter) allowed us to gather single-nAChR photobleaching measurements without interference from intracellular fluorescence. Thus, an additional advantage of the ZMW arrays used in these measurements is the ability to choose a ZMW diameter appropriate to the receptor density. Comparing bleaching steps of $\alpha 4$ -GFP yielded 2-step bleaching in 52% of the ZMWs (Figure 4). This confirms previous suggestions, based on indirect measurements, that plasma membrane $(\alpha 4)_3(\beta 2)_2$ and $(\alpha 4)_2(\beta 2)_3$ nAChRs exist in roughly similar numbers^{13,35}—quite different from the measurements with $\alpha 4\beta 4$ nAChRs which heavily favored the stoichiometry with three $\alpha 4$ subunits.

After upregulation of plasma membrane $\alpha 4\beta 2$ nAChRs by 24 h of exposure to nicotine (500 nM) or cytosine (500 nM), we found, as expected, more frequent single-molecule events (~10% of PM-mCherry ZMWs), even in ~144 nm diameter ZMWs. Interestingly, these two drugs produced significantly different effects on nAChR stoichiometry: 60% $(\alpha 4)_2(\beta 2)_3$ for nicotine but only 38% for cytosine (Figure 4). This confirmed

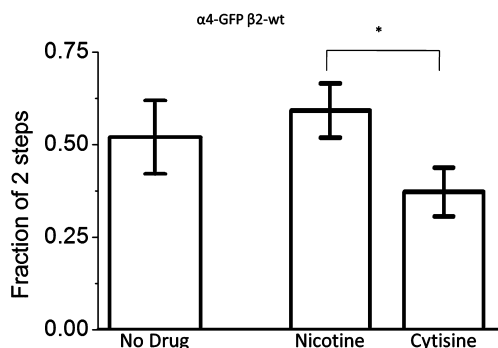


Figure 4. Stoichiometry of $\alpha 4\beta 2$ receptors. Fraction of the informative wells exhibiting 2 bleaching steps for $\alpha 4$ -GFP + $\beta 2$ -wt exposed to no drug ($n = 81$), nicotine ($n = 179$), and cytosine ($n = 117$). The error bars show the relative standard error of the mean of the wells exhibiting two-step bleaching. *, significant at $P < 0.05$.

that nicotine induced the preferential transport of the $(\alpha 4)_2(\beta 2)_3$ stoichiometry to the plasma membrane.^{30,33,34} In contrast, cytosine induced a plasma membrane population favoring the $(\alpha 4)_3(\beta 2)_2$ stoichiometry. This effect of cytosine is consistent with measurements that cytosine activates nAChRs formed by microinjecting *Xenopus* oocytes with more $\alpha 4$ than $\beta 2$ cRNA³⁴ as well as with very recent macroscopic FRET-based measurements of intracellular $\alpha 4\beta 2$ stoichiometry.³³ Thus, ZMW-based measurements of $(\alpha 4)_2(\beta 2)_3$ stoichiometry confirm several existing ideas but more importantly also extend our knowledge of pharmacological chaperoning to the single-molecule level. Additionally, the shift in stoichiometry of $\alpha 4\beta 2$ under different conditions indicates that there is no bias toward the trafficking of a particular stoichiometry to the terminal parts of filopodia.

The isolation of receptors in filopodia that have extended into ZMWs appears to limit the diffusion to such an extent that receptors can be imaged for tens of seconds. Similar experiments in HEK cells did not yield a similar confinement but instead resulted in only transient fluorescence (< 400 ms), indicating the diffusion of receptors in and out of the well. This suggests that the advantage of using cells that generate neurite-like projections, such as N2a cells, is that they can be optimized for interactions with nanostructures for the isolation of receptors.

Single-molecule experiments on membrane proteins have previously required very low densities of fluorophores. This can be accomplished with low, nonphysiological protein densities. Experiments with higher surface densities commonly use low-efficiency labeling of target proteins, but such schemes label only a small percentage of subunits preventing counting or full analysis within individual receptors. Due to concerns that artificially low concentrations of receptors, such as those in most single-molecule methods, can alter the dynamics of assembly and trafficking of receptors, we sought to develop the present method, allowing the isolation of proteins at physiological densities. We now show that the integration of ZMW nanostructures with N2a cells provides the capability to isolate individual receptors even at physiological membrane densities. We believe that ZMWs would be appropriate even at densities 10-fold greater than studied here.

At the opposite end of the density range, even rather sparse $\alpha 4\beta 2$ receptors are experimentally accessible with larger-diameter ZMWs. This technique provides the tools to study the properties of individual membrane receptors in living cells,

as controlled by pharmacological, pathological, and developmental processes. This technique could also provide the means to extend simultaneous single channel electrophysiology and fluorescence studies.³⁶ We believe that this integration of nanostructured devices with live cells can be widely applied to study a variety of membrane-resident proteins, including ion channels, transporters, and other receptors.

■ ASSOCIATED CONTENT

📄 Supporting Information

Detailed methods and supplemental figures. This material is available free of charge via the Internet at <http://pubs.acs.org>.

■ AUTHOR INFORMATION

Corresponding Author

*E-mail: lester@caltech.edu.

Notes

The authors declare the following competing financial interest(s): Jonas Korklach, Stephen W. Turner, and Khai Luong are full-time employees of Pacific Biosciences Inc., a company commercializing single-molecule, real-time detection technologies.

■ ACKNOWLEDGMENTS

We thank A. Fernandez and M. Boitano for assistance in preparing ZMW arrays. Supported by a Beckman Fellowship and an NIH NRSA to C.I.R., by a California Tobacco-Related Disease Research Fellowship to R.S., and by the US National Institutes of Health (NS34407).

■ REFERENCES

- (1) Sako, Y.; Minoghchi, S.; Yanagida, T. *Nat. Cell Biol.* **2000**, *2* (3), 168–172.
- (2) Betzig, E.; Patterson, G. H.; Sougrat, R.; Lindwasser, O. W.; Olenych, S.; Bonifacino, J. S.; Davidson, M. W.; Lippincott-Schwartz, J.; Hess, H. F. *Science* **2006**, *313* (5793), 1642–5.
- (3) Dani, A.; Huang, B.; Bergan, J.; Dulac, C.; Zhuang, X. W. *Neuron* **2010**, *68* (5), 843–856.
- (4) Kim, S. Y.; Miller, E. J.; Frydman, J.; Moerner, W. E. *J. Mol. Biol.* **2010**, *401* (4), 553–563.
- (5) Kelly, Christopher, V.; Baird, Barbara, A.; Craighead, Harold, G. *Biophys. J.* **2011**, *100* (7), L34–L36.
- (6) Iyer, G.; Michalet, X.; Chang, Y.-P.; Pinaud, F. F.; Matyas, S. E.; Payne, G.; Weiss, S. *Nano Lett.* **2008**, *8* (12), 4618–4623.
- (7) Taraska, J. W.; Zagotta, W. N. *Neuron* **2010**, *66* (2), 170–89.
- (8) Fernandes, C. C.; Berg, D. K.; Gomez-Varela, D. *J. Neurosci.* **2010**, *30* (26), 8841–8851.
- (9) Hille, B. *Ionic Channels of Excitable Membranes*; 3rd ed.; Sinauer: Sunderland, MA, 2001.
- (10) Ulbrich, M. H.; Isacoff, E. Y. *Nat. Meth.* **2007**, *4* (4), 319–21.
- (11) Pantoja, R.; Rodriguez, E. A.; Dibas, M. I.; Dougherty, D. A.; Lester, H. A. *Biophys. J.* **2009**, *96* (1), 226–37.
- (12) Simonson, P. D.; DeBerg, H. A.; Ge, P. H.; Alexander, J. K.; Jeyifous, O.; Green, W. N.; Selvin, P. R. *Biophys. J.* **2010**, *99* (10), L81–L83.
- (13) Srinivasan, R.; Pantoja, R.; Moss, F. J.; Mackey, E. D. W.; Son, C.; Miwa, J.; Lester, H. A. *J. Gen. Physiol.* **2011**, *137*, 59–79.
- (14) Moran-Mirabal, J. M.; Torres, A. J.; Samiee, K. T.; Baird, B. A.; Craighead, H. G. *Nanotechnology* **2007**, *18* (19), 5101.
- (15) Moran-Mirabal, J. M.; Craighead, H. G. *Methods* **2008**, *46* (1), 11–17.
- (16) Aouani, H.; Mahboub, O.; Bonod, N.; Devaux, E.; Popov, E.; Rigneault, H.; Ebbesen, T. W.; Wenger, J. *Nano Lett.* **2011**, *11* (2), 637–644.

- (17) Aouani, H.; Mahboub, O.; Devaux, E.; Rigneault, H.; Ebbesen, T. W.; Wenger, J. *Nano Lett.* **2011**, *11* (6), 2400–2406.
- (18) Levene, M. J.; Korlach, J.; Turner, S. W.; Foquet, M.; Craighead, H. G.; Webb, W. W. *Science* **2003**, *299* (5607), 682–686.
- (19) Edel, J. B.; Wu, M.; Baird, B.; Craighead, H. G. *Biophys. J.* **2005**, *88* (6), L43–5.
- (20) Wenger, J.; Conchonaud, F.; Dintinger, J.; Wawrezynieck, L.; Ebbesen, T. W.; Rigneault, H.; Marguet, D.; Lenne, P. F. *Biophys. J.* **2007**, *92* (3), 913–9.
- (21) Graham, A. J.; Ray, M. A.; Perry, E. K.; Jaros, E.; Perry, R. H.; Volsen, S. G.; Bose, S.; Evans, N.; Lindstrom, J.; Court, J. A. *J. Chem. Neuroanat.* **2003**, *25* (2), 97–113.
- (22) Tapia, L.; Kuryatov, A.; Lindstrom, J. *Mol. Pharmacol.* **2007**, *71* (3), 769–76.
- (23) Miwa, J. M.; Freedman, R.; Lester, H. A. *Neuron* **2011**, *70* (1), 20–33.
- (24) Xiao, C.; Srinivasan, R.; Drenan, R. M.; Mackey, E. D. W.; McIntosh, J. M.; Lester, H. A. *Biochem. Pharmacol.* **2011**, *82* (8), 852–861.
- (25) Richards, C. I.; Srinivasan, R.; Xiao, C.; Mackey, E. D. W.; Miwa, J. M.; Lester, H. A. *J. Biol. Chem.* **2011**, *286* (36), 31241–31249.
- (26) Ji, W.; Xu, P.; Li, Z.; Lu, J.; Liu, L.; Zhan, Y.; Chen, Y.; Hille, B.; Xu, T.; Chen, L. *Proc. Natl. Acad. Sci. U.S.A.* **2008**, *105* (36), 13668–73.
- (27) Kawate, T.; Michel, J.; Birdsong, W.; Gouaux, E. *Nature* **2009**, *460* (7255), 592–598.
- (28) Marks, M. J.; Burch, J. B.; Collins, A. C. *J. Pharmacol. Exp. Ther.* **1983**, *226* (3), 817–25.
- (29) Schwartz, R. D.; Kellar, K. J. *J. Neurochem.* **1985**, *45* (2), 427–33.
- (30) Buisson, B.; Bertrand, D. *J. Neurosci.* **2001**, *21* (6), 1819–29.
- (31) Kuryatov, A.; Luo, J.; Cooper, J.; Lindstrom, J. *Mol. Pharmacol.* **2005**, *68* (6), 1839–51.
- (32) Sallette, J.; Pons, S.; Devillers-Thiery, A.; Soudant, M.; Prado de Carvalho, L.; Changeux, J. P.; Corringier, P. J. *Neuron* **2005**, *46* (4), 595–607.
- (33) Srinivasan, R.; Richards, C. I.; Xiao, C.; Rhee, D.; Pantoja, R.; Dougherty, D. A.; Miwa, J. M.; Lester, H. A. *Mol. Pharmacol.* **2012**, *81* (6), 759–69.
- (34) Moroni, M.; Zwart, R.; Sher, E.; Cassels, B. K.; Bermudez, I. *Mol. Pharmacol.* **2006**, *70* (2), 755–68.
- (35) Nelson, M. E.; Kuryatov, A.; Choi, C. H.; Zhou, Y.; Lindstrom, J. *Mol. Pharmacol.* **2003**, *63* (2), 332–41.
- (36) Schmauder, R.; Kosanic, D.; Hovius, R.; Vogel, H. *ChemBioChem* **2011**, *12* (16), 2431–2434.